Two-Step Spin Conversion of [Fe^{II}(5-NO_2-sal-N(1,4,7,10))]: 292, 153, and 103 K X-ray Crystal and Molecular Structure and Infrared, Magnetic, Mössbauer, Calorimetric, and Theoretical Studies

Didier Boinnard,[†] Azzedine Bousseksou,[†] Ary Dworkin,[‡] Jean-Michel Savariault,[§] François Varret,[∥] and Jean-Pierre Tuchagues*,[†]

Laboratoire de Chimie de Coordination du CNRS, UP 8241 liée par conventions à l'Université Paul Sabatier et à l'Institut National Polytechnique, 205 route de Narbonne, 31077 Toulouse Cedex, France, Laboratoire de Chimie Physique des Matériaux Amorphes, UA CNRS D1104, Université de Paris-Sud, 91405 Orsay Cedex, France, Centre d'Elaboration des Matériaux et d'Etudes Structurales du CNRS, 29 rue Jeanne Marvig, 31055 Toulouse Cedex, France, and Département de Recherches Physiques, UA CNRS 71, Université Pierre et Marie Curie, 75252 Paris Cédex, France

Received August 27, 1993[⊗]

A detailed study of the two-step spin-state conversion in [Fe^{II}(5-NO_2-sal-N(1,4,7,10))] is presented with special emphasis on the structural changes evidenced by a multitemperature X-ray crystal and molecular structure study (292, 153, 103 K). The ligand (5-NO_2-sal-N(1,4,7,10)) results from the Schiff base condensation of 5-nitrosalicylaldehyde with tetraazadecane in a 2:1 ratio. The title molecule crystallizes in the monoclinic system, space group $P2/c$, with $Z = 2$ and $a = 10.153(1)$ Å, $b = 8.490(3)$ Å, $c = 13.173(2)$ Å, and $\beta = 109.93(2)°$ at 292 K. At 153 K, the space group of the monoclinic system is $P2$ with $Z = 2$ and $a = 9.952(1)$ Å, $b = 8.537(2)$ Å, $c = 13.070(1)$ Å, and $\beta = 109.47(1)°$, and at 103 K, the crystalline system is triclinic, space group $P1$, with $Z = 2$ and $a = 9.839(3)$ Å, $b = 8.336(4)$ Å, $c = 13.066(6)$ Å, $\alpha = 90.06(3)°$, $\beta = 107.84(3)°$, and $\gamma = 90.01(2)°$. The structures were solved by the heavy-atom method and refined to conventional agreement indices $R = 0.052$ (292 K), $R = 0.055$ (153 K), and $R = 0.092$ (103 K). The structures consist of [Fe^{II}(5-NO_2-sal-N(1,4,7,10))] complex molecules linked into infinite chains through two sets of N–H···O(nitro) hydrogen bonds, the central iron atom of each molecule being coordinated to the six donor atoms of the dianion of the N_4O_2 ligand. Two $S = 2 \leftrightarrow S = 0$ spin-state conversions involving each ~50% of the molecules occur in the same temperature range as the two structural phase transitions which clearly allow one to distinguish two equally distributed sets of molecules in this material. The X-ray molecular structure determinations, corroborated by the low-temperature IR studies, also allow one to illustrate the role of intermolecular interactions in the cooperativeness of the spin-state conversion mechanism through modifications of the hydrogen bond network at each step of the spin-state conversion. The two discontinuities evidenced by the thermal dependence of the Mössbauer parameters, ΔE_Q^{HS} and ΔE_Q^{LS}, and area ratio, A_{HS}/A_{tot}, and magnetic susceptibility and differential scanning calorimetry allow one to confirm that the two steps of the spin-state conversion are associated with the structural phase transitions evidenced by the X-ray molecular structure determinations. The theoretical approach based on the Ising-like model modified to take into account the nonequivalence of the two sublattices, and its application to [Fe^{II}(5-NO_2-sal-N(1,4,7,10))], allows one to correctly account for the above-mentioned experimental observations, confirming that the origin of this unique experimental behavior must be related to the structural phase transitions.

Introduction

Among the compounds exhibiting a spin-state conversion, [Fe^{II}-(5-NO_2-sal-N(1,4,7,10))] exhibits unusual features: (i) mononuclear iron(II) in a hexadentate N_4O_2 ligand environment; (ii) spin conversion occurring in two rather abrupt steps separated by a ~35 K broad plateau characterized by the presence of ~50% of HS (high spin) and LS (low spin) molecules.

Examples of two-step spin-state conversions are scarce and limited to iron complexes with a predominance of iron(II)[1-4] over iron(III).[5] Among them, [Fe(2-picolylamine)$_3$]Cl_2·EtOH is the only compound that has been extensively investigated[6-22] by several methods including detailed single-crystal X-ray studies at several temperatures between 90 and 298 K. From this wide range of minutely detailed studies, Gütlich et al.[22-24] concluded that the

* To whom correspondence should be addressed.
† Laboratoire de Chimie de Coordination.
‡ Laboratoire de Chimie Physique des Matériaux Amorphes.
§ Centre d'Elaboration des Matériaux et d'Etudes Structurales.
∥ Département de Recherches Physiques.
⊗ Abstract published in *Advance ACS Abstracts*, December 15, 1993.

(1) Köppen, H.; Müller, E. W.; Köhler, C. P.; Spiering, H.; Gütlich, P. *Chem. Phys. Lett.* **1982**, *91*, 348.
(2) König, E.; Ritter, G.; Dengler, J.; Nelson, S. M. *Inorg. Chem.* **1987**, *26*, 3582.
(3) Figg, D. C.; Herber, R. H.; Felner, I.; *Inorg. Chem.* **1991**, *30*, 2535.
(4) Real, J. A.; Bolvin, H.; Bousseksou, A.; Dworkin, A.; Kahn, O.; Varret, F.; Zarembowitch, J. *J. Am. Chem. Soc.* **1992**, *114*, 4650.
(5) Zelentsov, V. V. *Sov. Sci. Rev. B, Chem.* **1987**, *10*, 485.
(6) Sorai, M.; Ensling, J.; Gütlich, P. *Chem. Phys.* **1976**, *18*, 199.
(7) Sorai, M.; Ensling, J.; Hasselbach, K. M.; Gütlich, P. *Chem. Phys.* **1977**, *20*, 197.
(8) Gütlich, P.; Link, R.; Steinhäuser, H. G. *Inorg. Chem.* **1978**, *17*, 2509.
(9) Greenaway, A. M.; Sinn, E. *J. Am. Chem. Soc.* **1978**, *100*, 1080.
(10) Gütlich, P.; Köppen, H.; Link, R.; Steinhäuser, H. G. *J. Chem. Phys.* **1979**, *70*, 3977.
(11) Katz, B. A.; Strouse, C. E. *J. Am. Chem. Soc.* **1979**, *101*, 6214.
(12) Mikami, M.; Konno, M.; Saito, Y. *Chem. Phys. Lett.* **1979**, *63*, 566.
(13) Greenaway, A. M.; O'Connor, C. J. Schrock, A.; Sinn, E. *Inorg. Chem.* **1979**, *18*, 2692.
(14) Mikami, M.; Konno, M.; Saito, Y. *Acta Crystallogr. B* **1980**, *36*, 275.
(15) Gütlich, P.; Köppen, H.; Steinhäuser, H. G. *Chem. Phys. Lett.* **1980**, *74*, 475.
(16) Meissner, E.; Köppen, H.; Spiering, H.; Gütlich, P. *Chem. Phys. Lett.* **1983**, *95*, 163.
(17) Meissner, E. Ph.D. Thesis, University of Mainz (Germany), 1984.
(18) Kaji, K.; Sorai, M. *Thermochim. Acta* **1985**, *88*, 185.
(19) Köppen, H. Ph.D. Thesis, University of Mainz (Germany), 1985.
(20) Wiehl, L.; Kiel, G.; Köhler, C. P.; Spiering, H.; Gütlich, P. *Inorg. Chem.* **1986**, *25*, 1565.
(21) Adler, P.; Wiehl, L.; Meissner, E.; Köhler, C. P.; Spiering, H.; Gütlich, P. *J. Phys. Chem. Solids* **1987**, *48*, 517.
(22) Gütlich, P. *Struct. Bonding* **1981**, *44*, 83.
(23) Köhler, C. P.; Jakobi, R.; Meissner, E.; Wiehl, L.; Spiering, H.; Gütlich, P. *J. Phys. Chem. Solids* **1990**, *51*, 239.
(24) Gütlich, P.; Hauser, A. *Coord. Chem. Rev.* **1990**, *97*, 1.

0020-1669/94/1333-0271$04.50/0

appearance of two steps calls for a cooperative spin-state conversion mechanism with long-range elastic interactions related to lattice effects. On the basis of heat capacity measurements, Sorai and Seki[25] interpreted the long-range character of these interactions as resulting from the coupling between the electronic state and the phonon system. It is also worth noticing that the theoretical approaches[26-28] made to account for two-step spin-state conversions proceed from a similar viewpoint.

However, as evidenced by König[29] in an exhaustive survey of the literature concerning the structural changes accompanying continuous or discontinuous (cooperative) spin-state transitions, and confirmed by the multitemperature structure studies reported since,[30-34] with the exception of $[Fe((C_2H_5)_2NC(S)S)_3]$[35] (as far as this compound can be considered to experience a continuous thermal spin-state conversion) and Nb_6I_{11} and its hydrogenated derivative, HNb_6I_{11},[36] the crystal does not change symmetry; or, more precisely, the space group symmetry of the two spin isomers is identical. The most important structural modifications observed, namely distances and angles within the coordination polyhedron around the metal atom, take place in the central part of the molecule while changes in the peripheral areas are usually small. However, the role played by intermolecular interactions, involving most often an extended hydrogen bond network, in the cooperative spin-transition mechanism has been documented in a very large number of cases.[24,29]

We present in this paper a detailed study of the two-step spin-state conversion in $[Fe^{II}(5\text{-}NO_2\text{-}sal\text{-}N(1,4,7,10))]$ with special emphasis on the structural changes evidenced by a multitemperature X-ray crystal and molecular structure study (103, 153, 292 K). The present study also includes variable-temperature IR spectroscopy, differential scanning calorimetry, and additional Mössbauer and variable-temperature magnetic susceptibility studies. The experimental results reported are analyzed within the framework of a recently proposed theoretical model.[28] A preliminary description of the two-step spin-state conversion observed in this ferrous mononuclear compound has been reported[37] as well as an account of its preparation and properties.[38]

Experimental Section

Materials and Ligand. 1,4,7,10-Tetraazadecane (N-1,4,7,10) was purchased from Fluka in high-purity grade and used as received. 5-Nitrosalicylaldehyde (Eastman) was sublimed prior to use. Iron acetate tetrahydrate was prepared in a Schlenk vessel under an atmosphere of purified nitrogen according to literature methods[39] and stored in an inert-atmosphere box (Vacuum Atmospheres H.E.43.2) equipped with a dry-train (Jahan EVAC 7). Solvents were distilled under nitrogen and degassed under vacuum prior to use. 5-NO_2-sal(N-1,4,7,10) was obtained as previously described.[40]

Complexes. Due to the oxygen sensitivity of the starting iron(II) acetate, all reactions were performed under an atmosphere of purified nitrogen by using Schlenk techniques. The general method of preparation was adapted from that described for the parent manganese(II) complexes.[40]

Fe(5-NO_2-sal-N(1,4,7,10))·*x*MeOH (1). Dark blue-green to black microcrystalline samples of the methanol solvate were prepared by reacting a methanolic solution of the ligand with a methanolic solution of ferrous acetate ($0.5 \leq x \leq 1$).

Fe(5-NO_2-sal-N(1,4,7,10))·*x*EtOH (2). Microcrystalline samples of the ethanol solvate were prepared by reacting ethanolic solutions of the ligand and of ferrous acetate ($0.5 \leq x \leq 1$).

Fe(5-NO_2-sal-N(1,4,7,10)) (3). Microcrystalline samples of the unsolvated complex were prepared by reacting solutions of the ligand in THF and ferrous acetate in methanol. Crystals of **3** were similarly obtained by slow interdiffusion of solutions of the ligand and ferrous acetate.

The analytical results for complexes **1–3** are in good agreement with the theoretical values for C, H, N, and Fe.

Physical Measurements. Element analyses were carried out at the microanalytical laboratory of the Laboratoire de Chimie de Coordination for C, H, and N and at the Service Central de Microanalyses du CNRS in Vernaison, France, for Fe. IR spectra were recorded on a Perkin-Elmer 983 spectrophotometer coupled with a Perkin-Elmer infrared data station. Samples were run as CsBr pellets prepared under nitrogen in the drybox. Variable-temperature IR spectra (300-100 K) were obtained with a 21500 SPECAC IR cell (KBr windows) mounted on the spectrophotometer, the thermal scanning being monitored by a homemade servocontrol device (±1 K accuracy).

Variable-temperature magnetic susceptibility data were obtained as previously described[41] on polycrystalline samples with a Faraday type magnetometer equipped with a continuous-flow Oxford Instruments cryostat.

Mössbauer measurements were obtained on a constant-acceleration conventional spectrometer with a 25 mCi source of ^{57}Co (Rh matrix). Isomer shift values (δ) throughout the paper are given with respect to metallic iron at room temperature. The absorber was a sample of 150 mg of microcrystalline powder of **1** enclosed in a 2-cm-diameter cylindrical plastic sample holder, the size of which had been determined to optimize the absorption. Variable-temperature spectra were obtained in the 300-80 K range, by using a MD 306 Oxford cryostat, the thermal scanning being monitored by an Oxford ITC4 servocontrol device (±0.1 K accuracy). A least-squares computer program[42] was used to fit the Mössbauer parameters and determine their standard deviations of statistical origin (given in parentheses).

Differential scanning calorimetry (DSC) measurements were obtained with a Perkin-Elmer DSC-2C differential scanning calorimeter including a homemade low-temperature attachment.[43] The instrument was calibrated at solid cyclohexane transition and melting temperatures. The weight of the samples which were sealed in aluminum sample holders varied between 5 and 6 mg. All results were analyzed with the Perkin-Elmer TADS 3600 system.

The powder X-ray diagram of **1** was recorded at 293 K on a XRD3000TT SEIFERT diffractometer equipped with a diffracted beam monochromator using the Cu Kα wavelength (1.5418 Å). The sample was packed down in an aluminum holder of cylindrical shape, 20-mm diameter and 0.5-mm thickness. An angular θ range spanning from 2 to 25° was investigated through a step-scan process.

X-ray Crystal Structure Determinations of [Fe(5-NO_2-sal-N(1,4,7,-10))] (3). Crystals of complex **3** form as black lozenge-based prismatic tablets including a pyramid-shaped cavity at the center of one of the main faces. A radiocrystallographic study of these crystals showed them to be twinned. Small single crystals in the shape of elongated parallelepipeds were obtained by cutting the aforementioned twinned crystals. The selected crystal was an elongated prismatic tablet of approximate dimensions 0.32 × 0.08 × 0.1 mm. It was sealed on a glass fiber and mounted on an Enraf-Nonius CAD 4 diffractometer equipped with a

(25) Sorai, M.; Seki, S. *J. Phys. Chem. Solids* **1974**, *35*, 555.
(26) Zelentsov, V. V.; Lapouchkin, G. I.; Sobolev, S. S.; Shipilov, V. I. *Dokl. Akad. Nauk.* **1986**, *289*, 393.
(27) Sasaki, N.; Kambara, T. *Phys. Rev. B* **1989**, *40*, 2442.
(28) Bousseksou, A.; Nasser, J.; Linares, J.; Boukheddaden, K.; Varret, F. *J. Phys. I (Paris)* **1992**, *2*, 1381.
(29) König, E. *Prog. Inorg. Chem.* **1987**, *35*, 527.
(30) Timken, M. D.; Strouse, C. E.; Soltis, S. M.; Daverio, S. A.; Hendrickson, D. N.; Abdel-Mawgoud, A. M.; Wilson, S. R. *J. Am. Chem. Soc.* **1986**, *108*, 395.
(31) Kennedy, B. J.; McGrath, A. C.; Murray, K. S.; Skelton, B. W.; White, A. H. *Inorg. Chem.* **1987**, *26*, 483.
(32) Chang, H. R.; McCusker, J. K.; Toftlund, H.; Wilson, S. R.; Trautwein, A. X.; Winkler, H.; Hendrickson, D. N. *J. Am. Chem. Soc.* **1990**, *112*, 6814.
(33) Gallois, B.; Real, J. A.; Hauw, C.; Zarembowitch, J. *Inorg. Chem.* **1990**, *29*, 1152.
(34) Oshio, H.; Toriumi, K.; Maeda, Y.; Takashima, Y. *Inorg. Chem.* **1991**, *30*, 4252.
(35) Leipoldt, J. G.; Coppens, P. *Inorg. Chem.* **1973**, *12*, 2269.
(36) Imoto, H.; Simon, A. *Inorg. Chem.* **1982**, *21*, 308.
(37) Petrouleas, V.; Tuchagues, J. P. *Chem. Phys. Lett.* **1987**, *137*, 21.
(38) Rakotonandrasana, A.; Boinnard, D.; Savariault, J. M.; Tuchagues, J. P.; Petrouleas, V.; Cartier, C.; Verdaguer, M. *Inorg. Chim. Acta* **1991**, *180*, 19.
(39) Rhoda, N.; Fraioli, A. V. *Inorg. Synth.* **1953**, *4*, 159.
(40) Mabad, B.; Cassoux, P.; Tuchagues, J. P.; Hendrickson, D. N. *Inorg. Chem.* **1986**, *25*, 1420.
(41) Luneau, D.; Savariault, J. M.; Cassoux, P.; Tuchagues, J. P. *J. Chem. Soc., Dalton Trans.* **1988**, 1225.
(42) Varret, F. *Proceedings of the International Conference on Mössbauer Effect Applications*, Jaipur, India, 1981; Indian National Science Academy: New Delhi, 1982..
(43) Dworkin, A.; Jaffré, J.; Szwarc, H. *Rev. Sci. Instrum.* **1991**, *62*, 1654.

Table 1. Crystallographic Data for [Fe^{II}(5-NO_2-sal-N-1,4,7,10)] ($FeC_{20}H_{22}N_6O_6$)

	temp (K)		
	103	153	292
fw	498.28	498.28	298.28
space group	*P*1 (No. 1)	*P*2 (No. 3)	*P*2/*c* (No.13)
a(Å)	9.839(3)	9.952(1)	10.153(1)
b(Å)	8.336(4)	8.537(2)	8.490(3)
c(Å)	13.066(6)	13.070(1)	13.173(2)
α (deg)	90.06(3)		
β (deg)	107.84(3)	109.47(1)	109.93(2)
γ (deg)	90.01(2)		
V (Å^3)	1020.2(5)	1046.9(3)	1067.6(4)
Z	2	2	2
λ(Mo Kα) (Å)	0.710 73	0.710 73	0.710 73
ρ_{calc} (g/cm^3)	1.62	1.58	1.55
μ (cm^{-1})	7.5	7.1	7.0
$R(F_o)^a$	0.092	0.055	0.052
$R_w(F_o)^b$	0.101	0.056	0.058

^{a} $R = (\Sigma||F_o| - |F_c||)/(\Sigma|F_o|)$. ^{b} $R_w = (\Sigma w^{1/2}||F_o| - |F_c||)/(\Sigma w^{1/2}|F_o|)$.

NJET variable-temperature accessory based on the cold N_2 gas stream method. The temperature was controlled before and after data collection by using KDP crystals of well-known phase transition temperatures (KHDP, 211.9 K; KD_2P, 122.4 K). According to these calibrations, the fluctuations in temperature were less than 1 K, although larger temperature variations resulted from temporary freezing of the crystal during the 103 K data collection. Cell constants were obtained at 292, 153, and 103 K from least-squares fits of 25 reflections in the 8.4–13.0 θ Mo Kα range. Parameters of crystal and intensity measurements are summarized in Table 1. Totals of 3461 (292 K), 1984 (153 K), and 6532 (103 K) unique reflections corresponding to a 2θ (Mo Kα) maximum of 70, 50, and 70°, respectively, were recorded by procedures described elsewhere[44] and corrected for Lorentz and polarization effects.[45] As a result of the above-mentioned size and shape of the crystal, it has been possible to use only 1352 (292 K), 1041 (153 K), and 1379 (103 K) reflections with $I > 3\sigma(I)$ for the structure determinations.

Structure Solution and Refinement. The unit cell parameters reported in Table 1 evidence an increase of *b* when the temperature is lowered from 292 to 153 K, while *a* and *c* experience a decrease. On further lowering of the temperature down to 103 K, the most important change is a decrease of β from 109.47 to 107.84°. This quite large β variation is accompanied by a small departure of α (90.06°) from the strictly right angle of the monoclinic high-temperature unit cell. Consequently, the unit cell is triclinic at 103 K.

At 292 K, an examination of the systematic extinctions affords the *Pc* or *P*2/*c* space groups. A subsequent statistical study of the reflections evidencing a symmetry center indicates the actual space group is *P*2/*c*. The 292 K structure was solved by using the heavy-atom method.[46] A succession of difference Fourier syntheses and least-squares refinements revealed the positions of all non-hydrogen atoms. At this stage, to take into account the elongated shape of the crystal, an absorption correction was applied to the data using the numerical method of Walker and Stuart.[47] All atoms were then given anisotropic temperature factors, and a subsequent difference Fourier synthesis revealed the positions of all hydrogen atoms. The hydrogen atoms were then included in the final refinement coupled to their bonded atoms at a fixed distance of 0.95 Å with a mean isotropic temperature factor.

At 153 K, the systematic extinctions previously observed at 292 K have vanished. Among the possible space groups, *P*2/*m*, *Pm*, and *P*2, only *P*2 is compatible with the 292 K space group, *P*2/*c*. Moreover, a statistical study of the reflections shows that the symmetry center is now lacking, in agreement with the properties of *P*2. The 153 K structure was solved by using the same methods as previously. However, the number of useful unique reflections with $I > 3\sigma(I)$ (1041) being quite small, bond length constraints have been introduced in the refinement procedure for intraligand bonds. An absorption correction was then applied to the data.[47] All atoms were then given anisotropic temperature factors. The hydrogen atoms were included in the final refinement coupled to their bonded atoms with a mean isotropic temperature factor as previously. For checking purpose, the determination of the 153 K structure has also been carried out in the space group of the 292 K structure (*P*2/*c*). Comparison of the R_G factors, as defined by Hamilton,[48] led to rejection of the centrosymmetric hypothesis at the 0.001 level. The final refinement afforded satisfactory equivalent isotropic thermal parameters for all atoms except for a discrepancy between the Λ and Δ iron atoms (U_{eq} = 0.0510(8) Å^2 (Fe_Λ) and 0.0054(4) Å^2 (Fe_Δ)). This discrepancy could arise either from spin-state fluctuations due to temperature variations during data collection or from a perturbation of the iron electron density resulting from the presence of two iron spin-states in the crystal. A careful examination of the intensities of the control reflections indicated that the first hypothesis could be discarded. In order to assess the validity of the second hypothesis, the structure factors for high-spin Fe^{2+} and low-spin Fe^{2+} were computed according to Fukamachi's method.[49] Slater's orbital-based wave functions with Clementi's coefficients[50] were used in the computation. The structure factors were then computed according to Van Dooren's numerical integration method in the 0–2 (sin θ)/λ range.[51] The numerical coefficients of the interpolation functions[52a,b] were then determined by least-squares methods. The structure factors for high-spin Fe^{2+} and low-spin Fe^{2+} obtained[53] were subsequently used to carry out a complete refinement of the 153 K data set. The final refinement afforded results identical to those previously obtained except for the thermal parameters of the iron atoms which had reasonable values and were of the same order of magnitude.[53]

At 103 K, as a consequence of the lower molecular symmetry, the number of variables has considerably increased while the number of significant observations has decreased; due to temperature instabilities, a large number of observations had to be discarded. Consequently, the structure solution and refinement could not be obtained by using classical methods. However, it was possible to solve and refine the 103 K structure by using the 153 K one as starting point. Thermal parameters were kept isotropic for all atoms. The results obtained from the final refinement (Table 1) are indicative of the problems encountered during the data collection and structure solution. The temperature instabilities show up through dispersion of the thermal parameters and their unexpectedly high values considering the data collection temperature.

The atomic scattering factors used were those proposed by Cromer and Waber[52b] with anomalous dispersion effects.[52c] Information pertinent to the physical properties of the crystal and the data collections and refinements is summarized in Table 1 and fully reported in the supplementary material. All calculations were performed on an Alliant VFX 80 computer using the programs SHELX 76,[54] SHELX 86,[46] and ORTEP.[55] The [Fe^{II}(5-NO_2-sal-N(1,4,7,10))] molecules at 292, 153, and 103 K are shown in Figures 1–4 with atom numbering. Selected bond lengths and angles are given in Table 2.

Results

The two-step spin-state conversion of Fe^{II}(5-NO_2-sal-N(1,4,7,-10)) was first observed and reported by two of us[37] for the methanol solvate **1**.[38] As all crystal growth experiments carried out with methanol as the unique solvent afforded microcrystalline samples unsuitable for X-ray diffraction, we explored the properties of other solvates and of unsolvated Fe^{II}(5-NO_2-sal-N(1,4,7,10)).

The spin-state conversion of the ethanol solvate **2** and the unsolvated compound **3** obtained according to the preparations described in the Experimental Section are almost identical to those of the methanol solvate **1**, as evidenced by variable-

(44) Mosset, A.; Bonnet, J. J.; Galy, J. *Acta Crystallogr., Sect. B: Struct. Crystallogr. Cryst. Chem.* **1977**, *B33*, 2639.
(45) Frentz, B. A. *SDP-Structure Determination Package*; Enraf-Nonius: Delft, Holland, 1982.
(46) Sheldrick, G. M. In *Crystallographic Computing 3*; Sheldrick, G. M., Krüger, C., Goddard, R., Eds.; Oxford University Press: Oxford, England, 1985; p 175.
(47) Walker, N.; Stuart, D. *Acta. Crystallogr., Sect. A: Found. Crystallogr.* **1983**, *A39*, 158.
(48) Hamilton, W. C. *Acta Crystallogr.* **1965**, *18*, 502.
(49) Fukamachi, T. *Technical Reports of I.S.S.P.*; Tokyo University: Tokyo, 1971; B series, No. 12.
(50) Clementi, E. Tables of Atomic Functions. *IBM J. Res. Developmt.* **1965**, *9*, No. 2.
(51) Van Dooren, P.; De Ridder, L. *J. Comput. Math.* **1976**, *2*, 207.
(52) Cromer, D. T.; Waber, J. T. *International Tables for X-ray Crystallography*; Kynoch Press: Birmingham, England, 1974; Vol. IV: (a) p 71; (b) Table 2.2.B, pp 99, 101; (c) Table 2.3.1, p 149.
(53) Supplementary material.
(54) Sheldrick, G. M. *SHELX 76. Program for Crystal Structure Determination*; University of Cambridge: Cambridge, England, 1976.
(55) Johnson, C. K. *ORTEP, Report ORNL-1794*; Oak Ridge National Laboratory: Oak Ridge, TN, 1965.

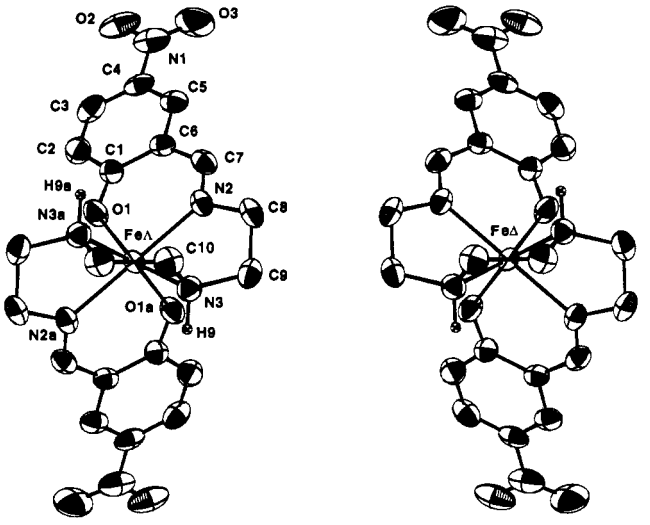

Figure 1. ORTEP view of the two [Fe^{II}(5-NO_2-sal-N(1,4,7,10))] molecules of the unit cell at 292 K.

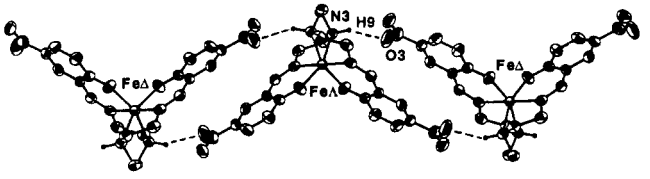

Figure 2. ORTEP view of a chain of hydrogen-bonded molecules of [Fe^{II}(5-NO_2-sal-N(1,4,7,10))] developing along [201] at 292 K.

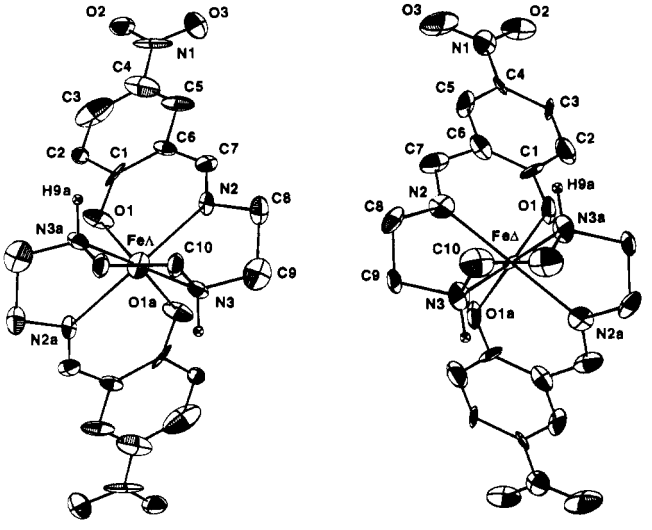

Figure 3. ORTEP view of the two [Fe^{II}(5-NO_2-sal-N(1,4,7,10))] molecules of the unit cell at 153 K.

temperature magnetic susceptibility studies carried out in the 80-280 K temperature range. The spin-state conversion temperatures are almost identical, the abruptness of the conversions is similar, and the ratio HS/LS molecules is ~50% on the plateau that extends similarly over ~35 K. The main observable difference is a small variation in the residual high-spin fraction (x_{HS}) below the LS–HS/LS–LS step that ranges 8–10% in **1**, 10–12% in **2**, and 13–15% in **3**. Several preparations of **1**–**3** have been subsequently carried out with slight modifications including ligand deprotonation and time and temperature of reaction. The residual x_{HS} below the LS–HS/LS–LS step is in the 8–16% range for all samples, and the variations seem to be related to preparative conditions like time and temperature of reaction as much as solvent. These results indicating that the cooperativeness of this particular spin-state conversion is independent of the crystallization solvent molecules, we were encouraged to grow crystals from mixtures including the solvents previously mentioned and finally succeeded to get crystals of **3** as described in the Experimental Section.

Molecular Structure of 3. The title molecule is comprised of a central iron atom coordinated to the six donor atoms of the dianion of the N_4O_2 ligand affording a coordination octahedron whose distortion varies with temperature, as discussed in the following.

The prominent features of the 292 K structure result from (i) the location of the iron on a 2-fold symmetry axis and (ii) the location of the inversion center between two adjacent molecules, which allows one to describe the unit cell (Z = 2) with half a molecule. However, due to the presence of a mirror plane between the two molecules of the unit cell, these are enantiomorphous as shown in the ORTEP representation of the unit cell sketched in Figure 1. The Δ and Λ enantiomorph molecules are defined with respect to the previously mentioned 2-fold symmetry axis joining the iron atom to the middle of the C10–C10a bond. The helicoid N_4O_2 ligand rotating along the 2-fold axis moves the Λ enantiomorph toward the observer (left-hand molecule of Figure 1) while it moves the Δ enantiomorph away from the observer (right-hand molecule of Figure 1). N3···O3 hydrogen bonds (3.057(7) Å) linking the central secondary amine function of each complex molecule to the terminal 5-nitro group of the neighboring molecule through the amine H9 atom (N3–H9···O3 = 153.4(5)°) afford infinite chains of doubly hydrogen-bonded complex molecules developing along [201] as shown in Figure 2. Consequently, each chain is made from alternate Λ and Δ molecules. The metal to ligand bond lengths reported in Table 2 (292 K) are typical of high-spin iron(II) coordinated to Schiff base ligands, while the LML angles indicate a particularly large distortion of the ferrous coordination octahedron.[38]

At 153 K, the inversion center has been lost, but each of the two iron atoms is on a 2-fold symmetry axis ($P2/c$ (292 K) → ($P2$ (153 K)) implying that the two molecules of the unit cell are different at this temperature. Furthermore, the ORTEP drawing of Figure 3 clearly shows that the two molecules of the unit cell are no more enantiomorphous as they have now different bond lengths and angles (Table 2, 153 K Λ and 153 K Δ columns) although they possess opposite helicities. Consequently, at 153 K, the [Fe^{II}(5-NO_2-sal-N(1,4,7,10))] molecules are evenly distributed into two sets differing not only in helicity but also in geometry, which could suggest that one set corresponds to the 50% of HS molecules while the other one would correspond to the 50% of LS molecules as the temperature of 153 K lies exactly in the middle of the 35 K plateau of the two-step spin conversion of this complex. Should this be true, the molecular structure determination would allow one to clearly distinguish the HS and LS spin isomers. A careful comparison of the 292 and 153 K similar molecules, including a superimposition of the ORTEP drawings, clearly shows that the Λ molecules are almost identical while the 153 K Δ molecules have slightly rotated counterclockwise with respect to the 292 K Δ molecules. These observations could agree with the fact that 50% of the molecules have converted to the LS form. At this point, we shall emphasize that, due to the molecular topology previously mentioned for the 292 K structure, the complex molecules are linked into infinite chains in an alternate way, namely, ···Λ molecule···Δ molecule···Λ molecule···Δ molecule··· through N3(Λ)···O3(Δ) hydrogen bonds (3.02(2) Å) and N3(Δ)···O3(Λ) ones (2.95(2) Å). There is thus an overall reduction in the intermolecular distances inside a chain (N3···O3 = 3.057(7) Å at 292 K) and a small tilting of the Δ molecules with respect to the Λ molecules. The crystal lattice can thus be viewed as including intertwinned sublattices of Λ and Δ molecules possibly coinciding with the LS and HS molecules.

However, a comparison of the metal to ligand bond lengths reported in Table 2 does not show any evidence of the significant reduction in bond length usually observed for a molecule

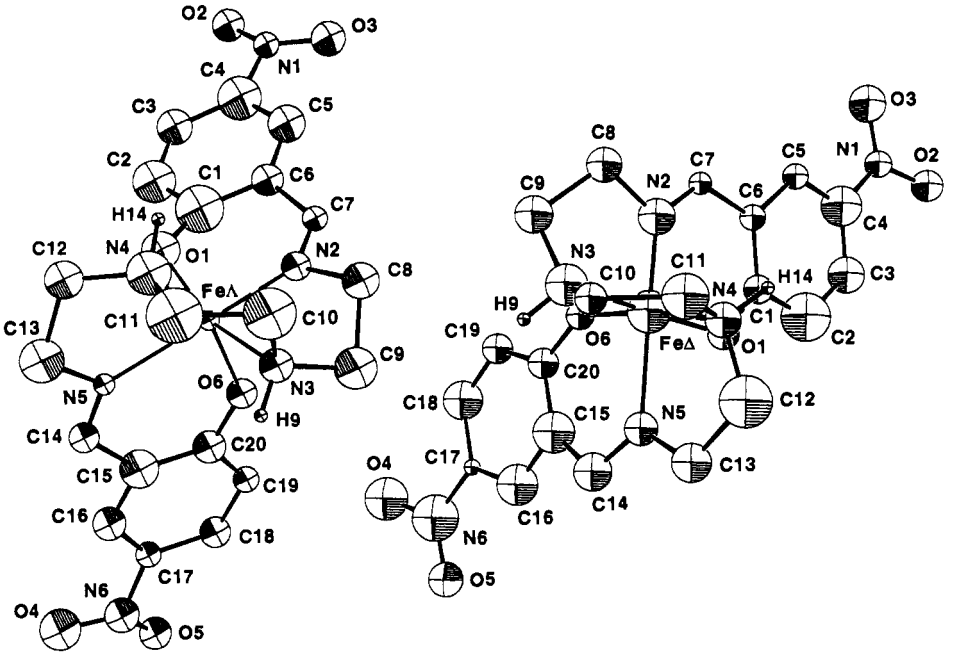

Figure 4. ORTEP view of the two [Fe^{II}(5-NO$_2$-sal-N(1,4,7,10))] molecules of the unit cell at 103 K.

Table 2. Selected Interatomic Distances (Å) and Angles for [Fe(5-NO$_2$-sal-N(1,4,7,10))] at 292 (HS), 153 (HS and LS), and 103 K (LS and LS)

	292 K	153 K			103 K	
	Δ,Λ	Λ	Δ		Λ	Δ
Fe–O1	2.041(4)	2.02(1)	2.07(1)	Fe–O1	2.07(3)	1.84(3)
Fe–N2	2.127(4)	2.16(1)	2.09(1)	Fe–N2	2.20(2)	1.75(3)
Fe–N3	2.235(4)	2.199(9)	2.25(1)	Fe–N3	2.08(4)	2.11(4)
Fe–N3a	2.235(4)	2.199(9)	2.25(1)	Fe–N4	2.13(4)	2.06(4)
Fe–N2a	2.127(4)	2.16(1)	2.09(1)	Fe–N5	1.83(3)	2.14(3)
Fe–O1a	2.041(4)	2.02(1)	2.07(1)	Fe–O6	2.03(3)	1.96(3)
O1–Fe–N2	86.0(2)	87.1(4)	85.4(4)	O1–Fe–N2	85(1)	100(1)
O1–Fe–N3	159.1(2)	159.7(4)	160.8(4)	O1–Fe–N3	160(1)	174(2)
O1–Fe–O1a	98.5(2)	95.0(4)	99.3(4)	O1–Fe–O6	99(1)	91(1)
O1–Fe–N2a	93.4(2)	92.2(4)	93.6(4)	O1–Fe–N5	99(1)	80(1)
O1–Fe–N3a	95.2(2)	95.5(4)	94.8(4)	O1–Fe–N4	97(1)	91(1)
N2–Fe–O1a	93.4(2)	92.2(4)	93.6(4)	N2–Fe–O6	90(1)	95(1)
N2–Fe–N2a	179.1(2)	178.9(3)	178.4(4)	N2–Fe–N5	175(1)	179(2)
N2–Fe–N3	77.4(2)	75.2(3)	80.7(4)	N2–Fe–N3	76(1)	80(2)
N2–Fe–N3a	103.3(2)	105.6(3)	100.6(4)	N2–Fe–N4	103(1)	91(2)
N3–Fe–O1a	95.2(2)	95.5(4)	94.8(4)	N3–Fe–O6	89(2)	96(2)
N3–Fe–N2a	103.3(2)	105.6(3)	100.6(4)	N3–Fe–N5	100(1)	100(1)
N3–Fe–N3a	76.7(2)	80.2(3)	74.9(4)	N3–Fe–N4	80(2)	83(2)
O1a–Fe–N2a	86.0(2)	87.1(4)	85.4(4)	O6–Fe–N5	93(1)	86(1)
O1a–Fe–N3a	159.1(2)	159.7(4)	160.8(4)	O6–Fe–N4	160(1)	173(10
N2a–Fe–N3a	77.4(2)	75.2(3)	80.7(4)	N4–Fe–N5	74(1)	88(1)
Fe–O1–C1	132.4(3)	131.0(7)	134.4(7)	Fe–O1–C1	132(2)	126(2)
Fe–N2–C7	127.4(3)	124.9(8)	130.0(8)	Fe–N2–C7	130(2)	123(2)
Fe–N2–C8	115.5(3)	118.2(7)	112.5(7)	Fe–N2–C8	117(2)	125(2)
Fe–N3–C9	105.1(3)	107.7(7)	102.6(6)	Fe–N3–C9	113(3)	104(3)
Fe–N3–C10	110.8(3)	110.7(6)	109.9(8)	Fe–N3–C10	105(3)	114(3)

experiencing a spin conversion from the HS to LS form. The average bond length for the 153 K Λ and Δ molecules is 2.126 and 2.137 Å, respectively, and the average bond length for both 153 K Λ and Δ molecules is 2.132 Å, the same value as the average bond length for the 292 K molecules (2.134 Å) within the experimental error. The observation of a change in distribution of the Fe–O, Fe–N(imine), and Fe–N(amine) bond lengths rather than an overall decrease of both types of Fe–N bonds is unprecedented and may cast some doubt on the occurrence of a spin conversion in the molecules of the specific crystal under X-ray diffraction study.

However, the indexation of the powder X-ray diagram of the sample of **1** studied with Mössbauer spectroscopy was successful with the cell dimensions of the single crystal used for the molecular structure determination. The cell parameters optimized from the Bragg angles are equal to those of the crystal. The observed reflections with their indexation and intensities compare very well[53] to the computed ones.[56] The observed and calculated intensities are in good agreement for all, except the first two, reflections, which can be attributed to a preferential orientation of the microcrystals resulting from the sample preparation. The agreement in the cell parameters and intensities of the reflections imply that the single crystal used for the molecular structure determination and the microcrystalline powder used for the physical measurements are the same compound crystallized in the same solid phase.

The slight difference in average bond length previously mentioned for the 153 K Λ and Δ molecules (2.126 and 2.137 Å, respectively) suggests that the iron of the Λ molecules is low-spin and the iron of the Δ molecules is high-spin. This hypothesis is confirmed by the comparison of the equivalent isotropic thermal parameters obtained for Fe$_\Lambda$ and Fe$_\Delta$ when the 153 K X-ray data are refined with iron structure factors corresponding to the following situations (cf. Structure Solution and Refinement section): (i) neutral iron for Fe$_\Lambda$ and Fe$_\Delta$ (U_{eq} (Å^2) = 0.0510(8) for Fe$_\Lambda$ and 0.0054(4) for Fe$_\Delta$); (ii) high-spin Fe^{2+} for Fe$_\Lambda$ for low-spin Fe^{2+} for Fe$_\Delta$ (U e$_q$ (Å^2) = 0.045(1) for Fe$_\Lambda$ and 0.0070-(7) for Fe$_\Delta$); (iii) low-spin Fe^{2+} for Fe$_\Lambda$ and high-spin Fe^{2+} for Fe$_\Delta$ (U_{eq} (Å^2) = 0.030(1) for Fe$_\Lambda$ and 0.0139(8) for Fe$_\Delta$). As shown in the Structure Solution and Refinement section, the difference in spin polarization originating in a different electronic distribution among the d orbitals for the $^5T_{2g}$ and $^1A_{1g}$ states is large enough to modify the iron atomic structure factors.[57] Consequently, when the modification of the iron structure factors due to this electronic polarization is ignored, *i.e.* when the structure

(56) Ivon, K.; Jeitschko, W.; Parthe, E. LAZY-PULVERIX: a computer program for calculating X-ray and neutron diffraction powder patterns. *J. Appl. Crystallogr.* **1977**, *10*, 73.

(57) An accurate electronic description for a metal ion including more than two valence electrons involved in a nonzero spin system requires one to take into account the spin polarization phenomenon (SP) which results in a multiplying term of the structure factor component associated with the inv olved electrons[65] and consequently an increase of the theoretical scattering factor f_{at} in the equation of the X-ray scattering of an atom, $f_{exp} = f_{at}$DW, where DW is the Debye–Waller factor (exp[$-(B_{eq}(\sin^2\theta)/\lambda^2)$]) ($f_{at}$ includes an invariable contribution from the core electrons and a contribution from the valence-shell electrons that depends on the oxidation state of the atom and electronic effects such as electron transfers or spin polarization (SP)).[66] In the case of iron(II), the SP term is dominated by the polarization of the electron density arising from a different filling up of the d orbitals involved in the low-spin and high-spin states, respectively.

factors of netural iron are taken for both Fe_Λ and Fe_Δ, a significant discrepancy in their thermal parameters ensues (i). When the structure factors of high-spin Fe^{2+} and low-spin Fe^{2+} are attributed to Fe_Λ and Fe_Δ, respectively, the discrepancy is still large (ii). On the contrary, when the structure factors of high-spin Fe^{2+} and low-spin Fe^{2+} are attributed to Fe_Λ and Fe_Δ, the thermal parameters are of the same order of magnitude (iii), which makes this attribution the most likely.

Taking into account all the aforementioned arguments, despite no significant reduction in bond length as usually observed for a molecule experiencing a spin conversion from the HS to LS state, we are finally led to consider that the iron of the Λ molecules experiences a HS to LS spin-state conversion between 292 and 153 K while the iron of the Δ molecules retains its HS state at 153 K. As none of the already reported iron(II) discontinuous spin-crossover compounds possesses oxygenated ligands and is characterized by a N_4O_2 coordination sphere, the absence of significant reduction in bond length at 153 K for the LS isomer of this atypical spin-state transition may originate in the presence of oxygen donors in the polydentate ligand and the alternance of directly hydrogen bonded HS and LS molecules.

As mentioned in the Experimental Section, the structure solution and refinement could not be obtained by using classical methods at 103 K as a consequence of the increased number of variables, due to the lower molecular symmetry, and the insufficient number of significant observations. Consequently, we will only comment about the general features resulting from the rough picture emerging from the solution and refinement leading to $R = 0.092$ and $R_w = 0.101$. At 103 K, the 2-fold symmetry axes of the 153 K structure have been lost ($P2$ (153 K) → ($P1$ (103 K)) implying that all atoms need be defined to describe the two molecules of the unit cell which results in appreciable changes in bond lengths and angles inside both molecules (Table 2, 103 K Λ and 103 K Δ columns). However, the ORTEP drawing of Figure 4 clearly shows that the two molecules of the unit cell still possess opposite helicities.

Comparison of the ORTEP drawings of the 153 and 103 K molecules clearly shows that the 103 K Λ molecule has rotated clockwise with respect to the 153 K Λ molecule while the 103 K Δ molecule has now reversed its rotation from counterclockwise (292 → 153 K) to clockwise (153 → 103 K) and considerably increased it. The four hydrogen bonds linking the central secondary amine functions of each complex molecule to the terminal 5-nitro groups of the neighboring molecules through the amine H atom are now different (N3···O11a = 3.14(5), N4···O9b = 3.30(5), O3···N10b = 2.65(5), O4···N9a = 3.01(5) Å). The average $N_{amine}\cdots O_{nitro}$ distance (3.02 Å) is intermediate between the 292 and 153 K ones, but there is a large tilting of the Δ molecules with respect to the Λ molecules in the direction opposite to that observed at 153 K.

The average metal to ligand bond length has decreased for both Λ (2.06 Å) and Δ (1.98 Å) molecules compared to the 153 K average bond length of the Λ and Δ molecules, 2.126 and 2.137 Å, respectively. The most important decrease (0.16 Å) concerns the Δ molecule supposed to be HS at 153 K, while the smaller decrease (0.07 Å) concerns the Λ molecule supposed to be already LS at 153 K. A general comparison of the average bond length for both Λ and Δ molecules between 292, 153, and 103 K affords 2.134 Å (100% HS), 2.132 Å (50% HS), and 2.02 Å (10% HS) that is an extrapolated bond length reduction of 0.13 Å for a 100% conversion from the HS to LS state. Although this average bond length change is among the smaller observed in the case of iron(II), it is in keeping with those reported for ferrous compounds including N_6 and P_4Br ligand sets.[29]

Infrared Spectroscopy. The 300 K IR spectra of KBr pellets including 1–5% of **1**–**3**, respectively, exhibit very similar absorption profiles over the 4000–400-cm^{-1} range, the main difference arising from the presence of a weak and broad ν_{OH} absorption around 3415 cm^{-1} in the spectra of **1** and **2**, which is not observable in the IR of **3**. Very few crystals of **3** being available, all absorptions in the corresponding IR spectrum were too weak to allow a reliable variable-temperature IR study. Consequently this study was undertaken with a microcrystalline sample of **1**, arising from the same preparation as the samples used for the other physical studies.

The most prominent observation concerns the absorptions arising from the ν_{NH} stretching vibrations of the secondary amino groups of the ligand. A very strong ν_{NH} absorption is present in all spectra, which slowly shifts from 3281 to 3272 cm^{-1} and decreases as the temperature is lowered between 300 and 102 K. At 175 K, a shoulder (3235 cm^{-1}) appears on the low-frequency side of this main absorption, which increases at the expense of the main absorption as the temperature is further lowered. Both absorptions have the same transmittance % at 102 K and have broadened, while the low-frequency absorption has slowly shifted down to 3229 cm^{-1}. This observation is perfectly consistent with the above-mentioned structural changes concerning the hydrogen bonds connecting the secondary amine functions to the nitro groups of adjacent molecules. While there is only one type of N3–H···O3 bond in the $P2/c$ high-temperature crystalline phase (3.057(7) Å), there are two types of hydrogen bonds, namely N3–H(Λ)···O3-(Δ) (3.02(2) Å) and N3–H(Δ)···O3(Λ) (2.95(2) Å) at 153 K, in the $P2$ intermediate-temperature crystalline phase. The broadening of both absorptions when the temperature is further lowered below 136 K may be related to the fact that there are four different hydrogen bonds in the $P1$ low-temperature crystalline phase.

Other significant changes, mainly in the M–L low-frequency region of the IR spectra, have been observed. However, no precise attribution has been attempted in the absence of isotopic substitution experiments.

Mössbauer Spectroscopy. A preliminary study of [Fe^{II}(5-NO_2-sal-N(1,4,7,10))] with γ absorption spectroscopy has been described in ref 37. A minutely detailed study of the thermal variation of the Mössbauer parameters of the sample of **1** used for the above-mentioned powder X-ray diffraction study is described hereafter. Representative Mössbauer spectra obtained on decreasing the temperature very slowly from 300 to 80 K, in order to avoid any hysteresis effect, are shown in Figure 5.

The low- and high-temperature spectra are characteristic of the low-spin and high-spin states of iron(II), respectively, with isomer shifts of 0.459(1) mm s^{-1} at 80 K and 0.958(2) mm s^{-1} at 300 K and quadrupole splittings of 0.966(2) mm s^{-1} at 80 K and 2.589(3) mm s^{-1} at 300 K. In the 180-100 K intermediate temperature range, the spectra consist of the HS and LS doublets in thermal equilibrium with each other. No spectrum deformation or line broadening is observable in this temperature range, indicating that the LS ↔ HS conversion rates are slow compared to the hyperfine frequencies (ca. 10^8 s^{-1}). At variance with the results obtained for {Fe(2,2′-bi-2-thiazoline)$(NCS)_2$}$_2$(2,2′-bipyrimidine),[4] there is no line broadening of the LS doublet at high temperature. Detailed values of the Mössbauer parameters resulting from least-squares fitting procedures are listed in Table 3 for a representative set of temperatures.

The thermal dependence of the area ratio A_{HS}/A_{tot} shown in Figure 6 clearly evidences a two-step spin conversion with a ~35 K plateau where an almost perfect spin-state equilibrium involving ~50% of HS and LS molecules is retained. The two steps of the conversion in the cooling mode are centered around 137 K (step 1) and 172.5 K (step 2). At variance with all previously described compounds exhibiting two-step spin-state conversions, step 2 is steeper than step 1 as clearly observable not only in Figure 6 but also in Figure 7, where the first derivative of the $\chi_M T$ product is plotted versus T (K). Below 110 K, the residual HS fraction is approximately 7% and does not decrease any more. It is well-known that the residual fractions, and particularly the HS one at low temperature, depend largely on the sample preparation.

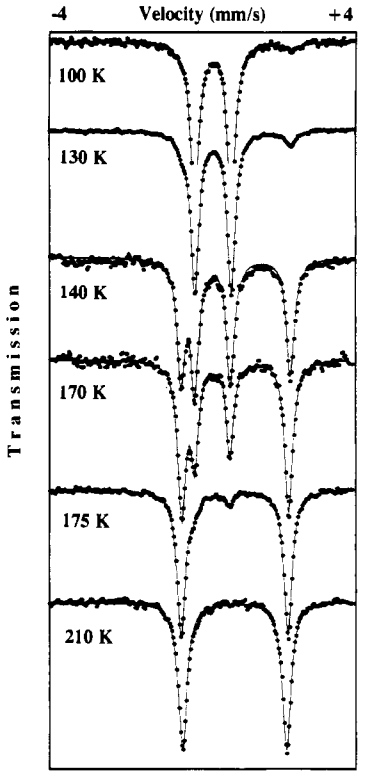

Figure 5. Selected Mössbauer spectra of [Fe^{II}(5-NO$_2$-sal-N(1,4,7,10))] obtained in the cooling mode between 300 and 80 K. The solid lines represent fitted curves.

Table 3. Representative Least-Squares-Fitted Mössbauer Data for [Fe^{II}(5-NO$_2$-sal-N(1,4,7,10))]^{a,b}

T (K)	low-spin state			high-spin state			$A_{HS}/A_{tot.}$ (%)
	δ	ΔE_Q^{LS}	$\Gamma/2$	δ	ΔE_Q^{HS}	$\Gamma/2$	
100	0.454(1)	0.961(1)	0.129(1)	1.040(6)	2.92(4)	0.23(3)	7.2(8)
130	0.448(3)	0.962(1)	0.128(1)	1.051(4)	2.856(7)	0.157(6)	10.27(3)
140	0.441(1)	0.930(2)	0.120(2)	1.053(1)	2.868(2)	0.128(2)	49.5(5)
150	0.442(1)	0.933(2)	0.120(2)	1.046(1)	2.856(3)	0.127(2)	52.1(4)
160	0.436(1)	0.932(1)	0.120(1)	1.040(1)	2.838(1)	0.130(1)	54.1(2)
170	0.429(2)	0.921(3)	0.112(2)	1.038(1)	2.815(2)	0.130(2)	64.7(5)
175	0.421(6)	0.92(1)	0.139(1)	1.034(1)	2.825(1)	0.132(1)	90.3(4)
180	0.39(2)	0.78(4)	0.139(1)	1.033(1)	2.812(2)	0.132(1)	97.3(5)
200				1.021(1)	2.781(2)	0.139(2)	100

^{a} δ = isomer shift (mm s^{-1}), ΔE_Q = quadrupole splitting (mm s^{-1}), $\Gamma/2$ = half-width of the lines, and $A_{HS}/A_{tot.}$ = area ratio of the high-spin doublet to the total area. ^{b} Statistical standard deviations are given in parentheses.

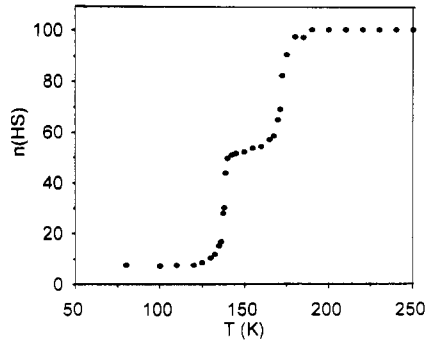

Figure 6. Temperature dependence of the area ratio $A_{HS}/A_{tot.}$ obtained from Mössbauer measurements of [Fe^{II}(5-NO$_2$-sal-N(1,4,7,10))] performed in the cooling mode.

On the other hand, the LS to HS spin-state conversion is complete above 190 K.

The values of $f_{LS,HS}$(80–135 K), $f_{LS,HS}$(137–171 K), and $f_{HS,HS}$(172.5–300 K) have been deduced from an analysis of the total area of the spectra obtained for the overall 80–300 K temperature range in the Debye approximation, including a thickness correction by a simple formula.[58,59] A subsequent study of the thermal variation of the recoil-free fraction of the system has been carried out through least-squares fitting procedures[60] allowing one to obtain the Debye temperatures Θ_D(LS,LS) = 157(5) K, Θ_D(LS,HS) = 154(2) K, and Θ_D(HS,HS) = 137(2) K. The temperature dependence of ln $A_{tot.}$, derived from the above-mentioned measurements, is displayed in Figure 8. The two steps of the spin transition induce appreciable discontinuities in the slope resulting from a change in the Debye temperature at each step. However, the discontinuity in the slope observed for step 1 is lesser than that observed for step 2.

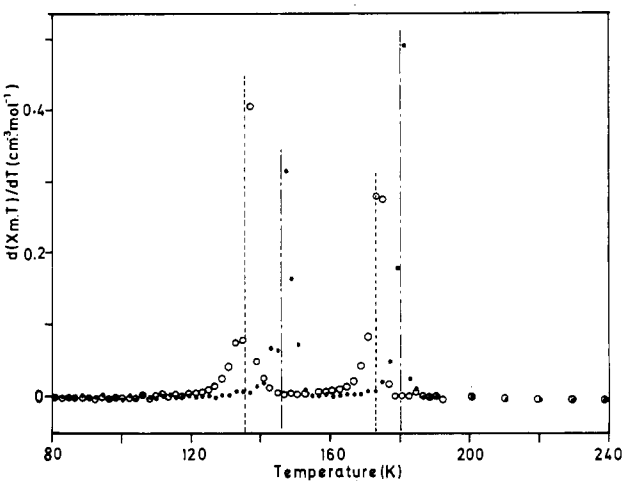

Figure 7. Thermal variation of the first derivative of $\chi_M T$ obtained from magnetic susceptibility measurements of [Fe^{II}(5-NO$_2$-sal-N(1,4,7,10))] carried out in the heating (•) and cooling (○) modes.

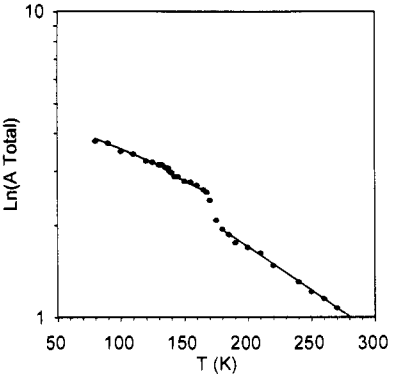

Figure 8. Temperature dependence of the area ratio ln $A_{tot.}$ obtained from Mössbauer measurements of [Fe^{II}(5-NO$_2$-sal-N(1,4,7,10))] performed in the cooling mode. The solid lines represent fitted curves.

The thermal variation of the quadrupole splitting of the high-spin doublet, ΔE_Q^{HS}, is shown in Figure 9. The large ΔE_Q^{HS} values (2.589(3)–2.92(4) mm s^{-1} between 300 and 100 K) indicate a local symmetry lower than cubic with a rather well-isolated ground orbital singlet. The small ΔE_Q^{HS} variation in this temperature range is characteristic of a strongly distorted octahedral environment as already evidenced by the X-ray crystal structure determination. It is possible to roughly assess the average energy δ of the excited orbital states belonging to the cubic triplet (insert in Figure 9) assuming that the ΔE_Q^{HS} slope varies as δ^{-1}.[61] The slope $d\Delta E_Q^{HS}/dT$ can be accurately determined by linear regression as $-1.118\ 10^{-3}$ mm s^{-1} K^{-1} yielding,

(58) Henry, M.; Teillet, J.; Varret, F. *Rev. Phys. Appl.* **1980**, *15*, 1095.
(59) Boukheddaden, K.; Varret, F. *Hyperfine Interact.* **1992**, *72*, 349.
(60) Claude, R.; Real, J. A.; Zarembowitch, J.; Kahn, O.; Ouahab, L.; Grandjean, D.; Boukheddaden, K.; Varret, F.; Dworkin, A. *Inorg. Chem.* **1990**, *29*, 4442.
(61) Ducouret-Cérèze, A.; Varret, F. *J. Phys. (Paris)* **1988**, *49*, 661.

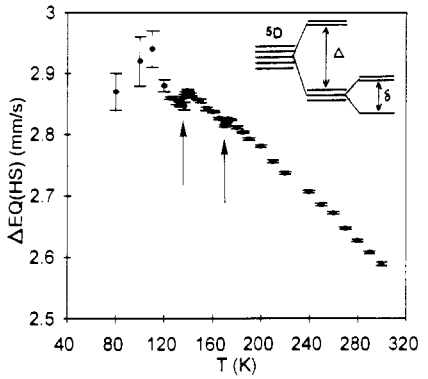

Figure 9. Thermal variation of the quadrupole splitting of the high-spin doublet obtained from Mössbauer measurements of [Fe^{II}(5-NO_2-sal-N(1,4,7,10))] carried out in the cooling mode. Error bars stand for statistical deviations, the arrows show the macroscopic steps of the spin-state conversion, and the insert depicts the ligand-field splittings of the HS state.

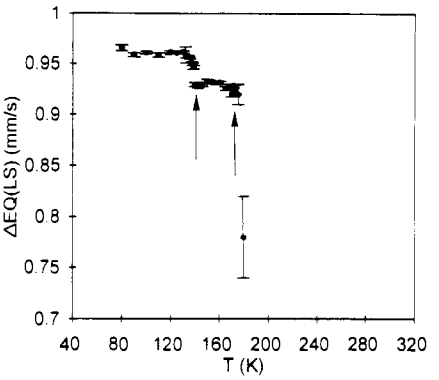

Figure 10. Thermal variation of the quadrupole splitting of the low-spin doublet obtained from Mössbauer measurements of [Fe^{II}(5-NO_2-sal-N(1,4,7,10))] carried out in the cooling mode. The arrows have the same meaning as in Figure 9.

as expected, a δ value (1529 cm^{-1}) much larger than that obtained for {Fe(2,2′-bi-2-thiazoline)$(NCS)_2$}$_2$(2,2′-bipyrimidine) (590 cm^{-1}).[4]

The thermal variation of ΔE_Q^{HS} exhibits two discontinuities around 135 and 175 K which disrupt a quasi linear overall shape. As observed for all previously studied parameters, these discontinuities are clearly associated with the two steps of the spin-state conversion. While the overall linearity of the thermal variation of ΔE_Q^{HS} is in keeping with that of previously studied iron(II) spin-crossover compounds,[4,60] the observation of two discontinuities is unprecedented and deserves some commments. In the case of {Fe(2,2′-bi-2-thiazoline)$(NCS)_2$}$_2$(2,2′-bipy),[4] ΔE_Q^{HS} ignores step 1 but detects step 2, which has been logically related by the authors to the larger sensitivity of ΔE_Q^{HS} to intramolecular versus intermolecular effects. In the case of the title mononuclear compound, the occurrence of steps 1 and 2 on adjacent molecules are both intermolecular events, which is reflected by the occurrence of ΔE_Q^{HS} discontinuities of the same order of magnitude (0.02–0.03 mm s^{-1}). Although, as expected, the amplitudes of both discontinuities are small compared to that detected for step 2 (intramolecular event) of the spin-state conversion of {Fe(2,2′-bi-2-thiazoline)$(NCS)_2$}$_2$(2,2′-bipy) (~0.1 mm s^{-1}), they are quite large compared to the amplitude of the discontinuity corresponding to step 1 (intermolecular event), which is hardly detectable in the same compound. These observations may be explained by considering the hydrogen-bond network evidenced by the X-ray molecular structure determination: Actually, the [Fe^{II}(5-NO_2-sal-N(1,4,7,10))] molecules are directly linked together into infinite chains involving four functional groups pertaining to the hexadentate ligand.

Such direct intermolecular interactions are much more efficient in propagating the effects of the coordination sphere distortions between adjacent iron centers than intermolecular interactions transmitted through hydrogen-bonded solvent molecules as it is usually the case.

The thermal variation of the quadrupole splitting of the low-spin doublet, ΔE_Q^{LS}, is shown in Figure 10. In keeping with the isotropic properties of the $^1A_{1g}$ electronic state, the ΔE_Q^{LS} values (0.78(4)–0.966(2) mm s^{-1} between 180 and 80 K) are significantly lower than the ΔE_Q^{HS} values, and their temperature dependence is rather small. However, the relatively large ΔE_Q^{LS} values confirm the high distortion of the iron local symmetry. Figure 10 clearly shows that the thermal variation of ΔE_Q^{LS} exhibits two discontinuities around 135 and 175 K. Although the 175 K discontinuity may be overestimated as the fraction of low-spin molecules is very small at this temperature (Table 3), each discontinuity is undoubtedly associated with the spin-conversion step occurring at the same temperature. These data are consistent with the usual assumption that ΔE_Q^{LS} is sensitive to intermolecular

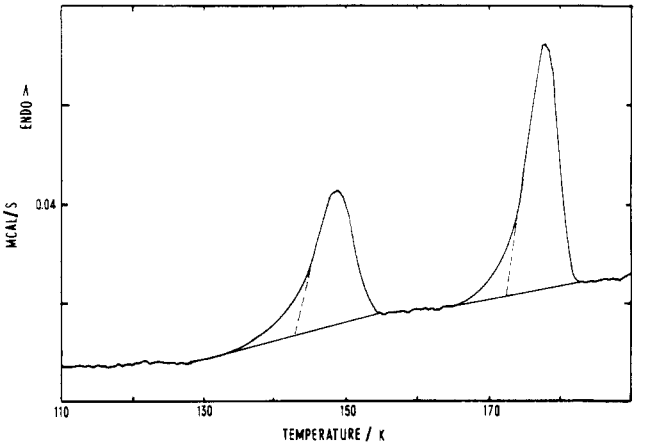

Figure 11. Differential scanning calorimetry curve obtained for [Fe^{II}(5-NO_2-sal-N(1,4,7,10))] in the heating mode, at a scan rate of 10 K min^{-1}.

effects through the lattice contribution. Indeed, the variation in ΔE_Q^{LS} at each step of the spin conversion would result from the fact that the HS and LS molecules have a different space group, as evidenced by the X-ray crystal structure determination, which is expected to afford a different lattice contribution. Again, these results are at variance with those described for {Fe(2,2′-bi-2-thiazoline)$(NCS)_2$}$_2$(2,2′-bipyrimidine), where the study of the thermal dependence of ΔE_Q^{LS} has led to the conclusion that the HS and LS phases have the same space group.[4]

Differential Scanning Calorimetry. Figure 11 shows a DSC scan of [Fe^{II}(5-NO_2-sal-N(1,4,7,10))], **1**, recorded with heating and cooling rates of 10 K min^{-1}. From this figure, the endothermic nature of the transitions is well established. The values of the transition temperatures obtained from the onset of the DSC peaks for the cooling and heating temperature sequences are 169.8 K (↓), 129.8 K (↓), 142.8 K (↑), and 172.3 K (↑). The width of the thermal hysteresis then follows as δT_c (171 K step) = 2.5 K and δT_c (136 K step) = 13 K. These values are in good agreement with the values obtained from the magnetic susceptibility measurements for the 136 K step (δT_c = 10 K). Although the agreement is not as good for the 171 K step (δT_c = 7 K), these results seem to indicate that not only both steps of the spin conversion correspond to first-order phenomena but moreover that the rate constant must be different for the two steps of the spin conversion.

The enthalpy changes, ΔH, associated with each step of the spin conversion have been obtained by averaging several measurements made for increasing and decreasing temperatures. The average values are 3.9 ± 0.5 kJ mol^{-1} (171 K step) and 2.6 ± 0.5 kJ mol^{-1} (136 K step). From the mean values (T_c↑ + T_c↓)/2, *i.e.* 171.1 and 136.3 K, the entrophy changes, ΔS, are 23 ± 3 J

mol^{-1} K^{-1} (171 K step) and 19 ± 3 J mol^{-1} K^{-1} (136 K step) indicating that both steps of this spin conversion are accompanied by equivalent entropy variations. Actually, considering the ~10% HS residual fraction remaining at temperatures lower than 130 K, the 171 K entropy change concerns 48% of the molecules while the 136 K entropy change concerns 42% of the molecules of the studied samples.

It is of interest to note that the experimental ΔS values gathered from the literature of spin-crossover complexes (86–48 J mol^{-1} K^{-1})[62] are larger than the sum of the ΔS obtained for both steps of the spin conversion of **1** (42 J mol^{-1} K^{-1}). However this sum is significantly larger than the entropy variation due to a change of the spin state alone, $\Delta S_{el.} = R \ln (\omega^5T_2 - \omega^1A_1) = R \ln 5 =$ 13.4 J mol^{-1} K^{-1}. The contribution by lattice vibrations being usually considered as minor, the additional contribution to ΔS should originate in the intramolecular vibration changes. These are associated with M–L stretching vibration and L–M–L deformation changes resulting in a molecular volume variation. Consequently, the molecular volume change associated with this spin conversion should be smaller than those previously determined for iron(II) spin-crossover complexes. As already shown in the X-ray crystal and molecular structure section, this inference is confirmed by the mean value of the M–L bond length variation (0.13 Å). A similar result (mean M–L bond length variation of 0.15 Å) had previously been obtained from the analysis of EXAFS spectra of **1**.[38] This result is probably related to the presence of a FeN_4O_2 core in [Fe^{II}(5-NO_2-sal-N(1,4,7,10))], while all previously reported Fe(II) spin-crossover complexes involve FeN_6 cores, with the exception of a FeP_4Br core.[29]

Theoretical Approach and Application to [Fe^{II}(5-NO_2-sal-N(1,4,7,10))]

A two-sublattices model, easily applicable to the present case, has been recently been proposed for the two-step spin conversion.[28] In this reported "Ising-like approach", the single molecule Hamiltonian $\mathcal{H}$ is $^1/_2$ $\Delta\sigma$, where σ is a fictitious spin operator with eigenvalues ±1 respectively associated with the HS and LS states. The degeneracies of the spin states, g_{HS} and g_{LS}, differ, due to the variation of electronic and vibrational properties upon spin conversion.[22] The crystal Hamiltonian written with the previously defined parameters[28] is

$$\mathcal{H} = \sum_i {}^1/_2\Delta_i\hat{\sigma}_i + \sum_{(ij)} J_{ij}\hat{\sigma}_i\hat{\sigma}_j \qquad (1)$$

where Δ_i is the energy difference between the two levels of the isolated site (i) and J_{ij} is a phenomenological interaction parameter between sites i and j. In ref 28, all molecules being considered as structurally equivalent, $\Delta_i = \Delta$, and their two-sublattices system involves three interaction parameters, J_A, J_B ("ferromagnetic"), and J_{AB} ("antiferromagnetic"). The mean-field treatment of the problem allowed one to qualitatively account for one-step and two-step spin conversions. This model was also applied to the spin-crossover system described in this paper. In the absence of structural data, the authors made the assumption of two equivalent sublattices and obtained the following parameters: $J_A = J_B =$ −280 K; $\Delta_A = \Delta_B =$ 920 K; $J_{AB} =$ 29 K.[28]

The aforementioned structural study suggests that sites A and B are not equivalent. Therefore, we apply the two-sublattices model in the most general case: $J_A \neq J_B$ and $\Delta_A \neq \Delta_B$. In a first step, we have considered a spin-conversion curve (Figure 12) corrected for hysteresis (by averaging the temperature values associated with a given value n_{HS} of the fraction of high-spin molecules) deduced from the magnetic measurements ($\chi_M = \chi_{dia} + (1 - n_{HS})\chi_{LS} + n_{HS}\chi_{HS}$) obtained for a powdered sample of **1**.[37] The parameters resulting from the fit are as follows: $\Delta_A =$ 880 K, $\Delta_B =$ 890 K, $J_A =$ −190 K, $J_B =$ −276 K, $J_{AB} =$ 45 K, and

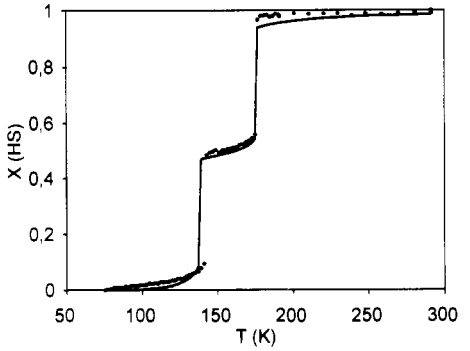

Figure 12. Thermal variation of the high-spin fraction n_{HS} of [Fe^{II}(5-NO_2-sal-N(1,4,7,10))]: (•) Experimental values obtained from magnetic susceptibility measurements in the heating and cooling modes and corrected for hysteresis; (—) least-squares fit.

$g_{HS}/g_{LS} = 400$. It is noteworthy that the nonequivalence of the sublattices ($J_A \neq J_B$ and/or $\Delta_A \neq \Delta_B$) could be anticipated from a careful comparison of the two steps of the experimental spin-conversion curve as the two-sublattices model allows one to predict that (i) in the case of equivalent sublattices ($J_A = J_B$ and $\Delta_A = \Delta_B$), the high-temperature step (2) is smoother than the low-temperature step (1) and (ii) in the case of discontinuous spin conversions, step 2 is of smaller amplitude than step 1. As shown by Figure 12, the theoretical results arising from the nonequivalent sublattices model allow one to account for the experimental data, while those arising from the equivalent sublattices model are clearly at variance with the experimental results.

Further independent confirmation of the nonequivalence of the sublattices comes out from the shape of the hysteresis loops, Figure 13a. The equivalent sublattices model allows one to predict two well-separated loops, while the nonequivalent sublattices model leads to separate branches in the plateau between the loops for the heating and cooling modes (Figure 13b). This arises obviously from the presence of different combinations of spin states on the plateau, A(HS)/B(LS) in the heating mode and A(LS)/B(HS) in the cooling mode, and affords direct evidence for the nonequivalence of the sublattices.

Free Energy, Entropy, and Heat Capacity. The entropy and heat capacity are calculated in the frame of the present model, using standard methods of statistical physics.[63] The calculated value for the entropy change per metal ion, 49 J mol^{-1} K^{-1} ($\Delta S \cong R \log(g_b/g_a)$, is in excellent agreement with the measured value, 42 ± 6 J mol^{-1} K^{-1}.

The heat capacity C is numerically derived from the entropy according to $C = T(dS/dT)$.

Figure 14 shows the theoretical thermal variation of the fraction n_{HS} of high-spin molecules and of the corresponding theoretical heat capacity C when the parameters J_A, J_B, J_{AB}, Δ_A, and Δ_B are chosen so that the free following situations result: (i) two-step spin-state conversion with step 1 steeper than step 2 (Figure 14a); (ii) two-step spin-state conversion with the same steepness for both steps (Figure 14b); (iii) two-step spin-state conversion with step 2 steeper than step 1 (Figure 14c). For all three situations, the thermal variation of the heat capacity C shows two peaks centered at the temperatures of the steps. In all three situations, there is a direct correlation between the steepness of each step and the sharpness of the corresponding heat capacity peak. This correlation is easily found in a two-level, one-sublattice model[28,64]

(62) König, E.; Ritter, G.; Kulshreshtha, S. *Chem. Rev.* **1985**, *85*, 219.
(63) Boccara, N. *Broken Symmetries, Theory of Transitions with Order Parameter*; Hermann: Paris, France, 1976.
(64) Bousseksou, A.; Nasser, J.; Linares, J.; Boukheddaden, K.; Varret, F. *J. Mol. Cryst. Liq. Cryst.* **1993**, *234*, 269.
(65) Becker, P.; Coppens, P. *Acta Crystallogr.* **1985**, *41A*, 177.
(66) Guinier, A. *Theory and Technique of X-ray Crystallography*; Dunod: Paris, France, 1956; p 510.

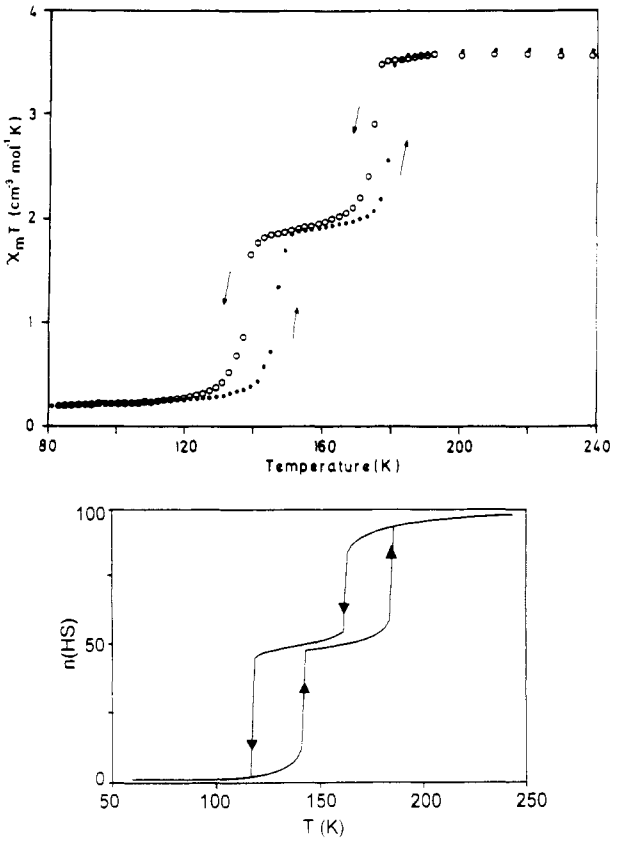

Figure 13. (a) Top: Temperature dependence of $\chi_M T$ obtained from magnetic susceptibility measurements of [Fe^{II}(5-NO_2-sal-N(1,4,7,10))] carried out in the heating (•) and cooling (○) modes (from ref 37). (b) Bottom: Theoretical temperature dependence of the fraction n_{HS} of high-spin molecules in the case of two first-order spin-state conversions, showing the hysteresis phenomenon obtained for the two nonequivalent sublattices situation.

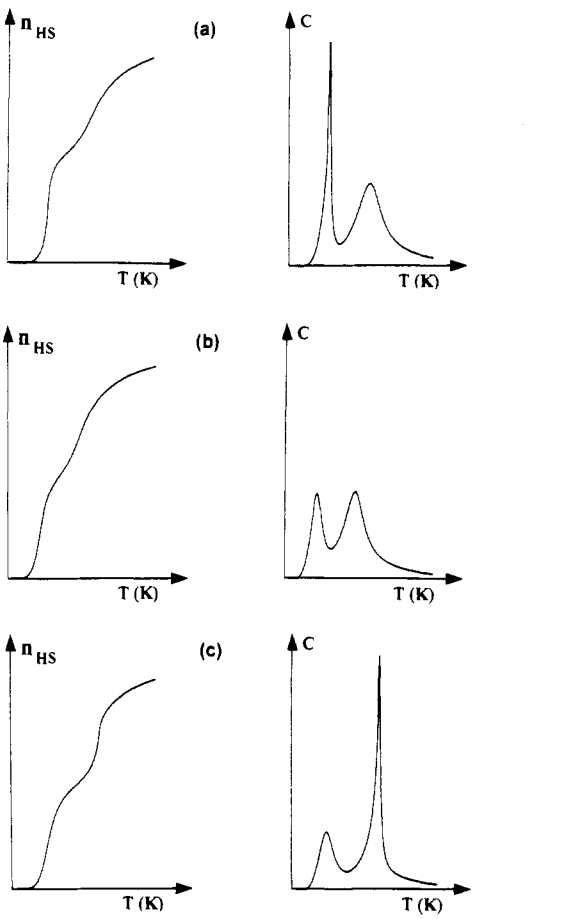

Figure 14. Theoretical temperature dependence of the fraction n_{HS} of high-spin molecules and corresponding theoretical heat capacity in the case of two-step spin-state conversions with (a) the low-temperature step (1) steeper than the high-temperature step (2), (b) the same steepness for both steps, and (c) step 2 steeper than step 1.

as the following:

$$C = Nk(J\langle\hat{\sigma}\rangle + \Delta/2)\, d\langle\hat{\sigma}\rangle/dT + Nk\Delta/2T\langle\hat{\sigma}\rangle + NkJ/T\langle\hat{\sigma}\rangle^2$$

where J is the "ferromagnetic" interaction. Such a correlation is indeed observed experimentally; *i.e.*, from the magnetic susceptibility measurements, step 2 of the spin-state conversion of **1** is steeper than step 1 and, from the DSC measurements, the heat capacity peak corresponding to step 2 is sharper than the heat capacity peak corresponding to step 1.

Conclusions

We have already pointed out that the thermally induced $^5T_{2g} \leftrightarrow {}^1A_{1g}$ spin-state conversion of [Fe^{II}(5-NO_2-sal-N(1,4,7,10))] exhibits unprecedented features: a mononuclear iron(II) center in a N_4O_2 ligand environment with spin conversion of discontinuous nature occurring in two steps separated by a 35 K broad spin equilibrium domain in which ca. 50% of HS and LS molecules coexist.[37]

The X-ray molecular structure determinations presented here allow one to confirm the mononuclear nature of [Fe^{II}(5-NO_2-sal-N(1,4,7,10))] and the presence of a N_4O_2 ligand environment around the ferrous ion. The N_4O_2 ligand set is thus associated, for the first time, with the spin-crossover phenomenon in a ferrous compound.

Moreover, these X-ray studies afford the first example of $S = 2 \leftrightarrow S = 0$ spin-state conversion associated with a characterized structural phase transition. Considering that two $S = 2 \leftrightarrow S = 0$ spin-state conversions involving each ~50% of the molecules occur in the same temperature range as the two structural phase transitions of this material, which clearly allow one to distinguish two equally distributed sets of molecules, it ensues that these two spin-state conversions result from the structural phase transitions as previously shown in the only case of Nb_6I_{11} and its hydrogenated derivative, HNb_6I_{11}.[36] However, at variance with Nb_6I_{11} and HNb_6I_{11}, which experience continuous spin-state conversions, [Fe^{II}(5-NO_2-sal-N(1,4,7,10))] exhibits two discontinuous HS ↔ LS conversions.

In accordance with the usual assumption that ΔE_Q^{LS} is sensitive to intermolecular effects through the lattice contribution, each discontinuity of the thermal variation of ΔE_Q^{LS} is undoubtedly associated with the spin-conversion step occurring at the same temperature. The variation in ΔE_Q^{LS} at each step of the spin conversion results from the fact that the HS and LS molecules have different symmetry properties, as evidenced by the X-ray crystal structure determination, which is expected to afford different lattice contributions.

The fact that changes in M–L bond lengths and L–M–L bond angles are moderate in this spin-crossover compound, in contrast with the larger bond lengths and bond angles changes evidenced for most other spin-crossover compounds, can be another aspect of the distinction between spin-crossover compounds exhibiting or not exhibiting a structural phase transition.[29] The moderate changes in M–L bond lengths and overall molecular volume associated with the spin-state conversions in [Fe^{II}(5-NO_2-sal-N(1,4,7,10))] are confirmed by the EXAFS[38] and calorimetric analysis, respectively.

The X-ray molecular structure determinations presented here also allow one to illustrate the role of intermolecular interactions in the cooperativeness of the spin-state conversion mechanism. As shown by Figure 2, the [Fe^{II}(5-NO_2-sal-N(1,4,7,10))] mol-

ecules are linked into infinite chains through two sets of N–H···O-(nitro) hydrogen bonds which are modified once at the spin-state conversion of 50% of the molecules and then at the spin-state conversion of the remaining HS molecules, as evidenced by the N···O distances and N–H···O angles modifications as well as the splitting of the ν_{NH} IR absorption.

The observation of two discontinuities (clearly associated with the steps of the spin-state conversion) in the thermal variation of ΔE_Q^{HS} may be explained by considering how the hydrogen-bond network links directly together the [Fe^{II}(5-NO_2-sal-N(1,4,7,-10))] molecules into infinite chains. Such direct intermolecular interactions are much more efficient in propagating the effects of the coordination sphere distortions between adjacent iron centers than intermolecular interactions transmitted through hydrogen-bonded solvent molecules as it is usually the case. Our present interpretation for this unprecedented observation is being thoroughly investigated through the study of the corresponding deuterated material.

The magnetic susceptibility and Mössbauer studies clearly show that step 2 is steeper than step 1 and the amplitude of step 2 is comparable to that of step 1, while the DSC experiments show that the heat capacity peak corresponding to step 2 is sharper than that corresponding to step 1. All these results are at variance with the observations made for all other two-step spin-state conversions. The theoretical approach based on the Ising-like model modified to take into account the nonequivalence of the two sublattices and its application to [Fe^{II}(5-NO_2-sal-N(1,4,7,-10))] allows one to take correctly into account all the above-mentioned experimental observations, confirming that the origin of this unique experimental behavior must be related to the structural phase transitions. We also observe that the Debye temperature variation of the ^{57}Fe nuclei of this compound follows a similar trend, as the Θ_D variation is larger for step 2 than for step 1. One of the questions that remain to be answered concerns the possible relationship between Θ_D and the steepness of a spin-state conversion.

Acknowledgment. A. Mari and G. Lemercier are acknowledged for their assistance in carrying out the magnetic susceptibility and Mössbauer measurements. We thank P. Becker for useful discussions concerning the analysis of the equivalent isotropic thermal parameters.

Supplementary Material Available: Tables giving crystal data and experimental details, atomic coordinates, anisotropic thermal parameters, hydrogen atom locations, and bond lengths and angles at 292, 153, and 103 K, atomic structure factors for high-spin Fe^{2+} and low-spin Fe^{2+} and coefficients for the analytical approximations to their scattering factors, powder X-ray diffraction data at 293 K, and complete 80–300 K least-squares-fitted Mössbauer data (19 pages). Ordering information is given on any current masthead page.